Refractive-Index-Based Screening of Membrane-Protein-Mediated Transfer across Biological Membranes

Magnus Brändén,[†*] Seyed R. Tabaei,[†] Gerhard Fischer,[‡] Richard Neutze,[‡] and Fredrik Höök[†*]
[†]Division of Biological Physics, Chalmers University of Technology, Gothenburg, Sweden; and [‡]Department of Chemistry, Biochemistry and Biophysics, University of Gothenburg, Gothenburg, Sweden

ABSTRACT Numerous membrane-transport proteins are major drug targets, and therefore a key ingredient in pharmaceutical development is the availability of reliable, efficient tools for membrane transport characterization and inhibition. Here, we present the use of evanescent-wave sensing for screening of membrane-protein-mediated transport across lipid bilayer membranes. This method is based on a direct recording of the temporal variations in the refractive index that occur upon a transfer-dependent change in the solute concentration inside liposomes associated to a surface plasmon resonance (SPR) active sensor surface. The applicability of the method is demonstrated by a functional study of the aquaglyceroporin PfAQP from the malaria parasite *Plasmodium falciparum*. Assays of the temperature dependence of facilitated diffusion of sugar alcohols on a single set of PfAQP-reconstituted liposomes reveal that the activation energies for facilitated diffusion of xylitol and sorbitol are the same as that previously measured for glycerol transport in the aquaglyceroporin of *Escherichia coli* (5 kcal/mole). These findings indicate that the aquaglyceroporin selectivity filter does not discriminate sugar alcohols based on their length, and that the extra energy cost of dehydration of larger sugar alcohols, upon entering the pore, is compensated for by additional hydrogen-bond interactions within the aquaglyceroporin pore.

INTRODUCTION

All cells are critically dependent on membrane proteins for uptake and release of metabolites, signal transduction, and energy conservation. Currently, the standard approaches for studying the membrane-protein-mediated transfer and the passive diffusion of uncharged molecules rely on measurements of osmotic-induced size changes of suspended lipid vesicles (so-called liposomes) (1), oocytes (2), or cells (3). These methods are based on light-scattering measurements of variations in scattered light intensity as the dimensions of the liposome (or cell-derived vesicle) change in response to osmotically induced water transfer across the lipid membrane. Upon exposure to a permeable analyte, the liposomes first shrink as water diffuses out of the liposomes, and subsequently swell as water reenters the liposomes driven by the inward permeation of the analyte molecules (4). Although this method has been successfully applied in numerous studies of passive and membrane-protein-mediated transfer of uncharged molecules (5), it is to some extent limited by the fact that a change in liposome size is a secondary and thus indirect effect that occurs in response to a change in osmolarity across the membrane. In addition, since not only the liposome size but also the liposome motion, analyte refractive index, and membrane aggregation may contribute to the intensity of the scattered light, the quantification of analyte transfer is generally not straightforward (6,7). Most of these limitations also apply for an alternative method in which osmotically induced liposome size variations are recorded by monitoring changes in self-quenching of liposome-entrapped fluorophores upon liposome shrinkage or swelling due to a concomitant increase or decrease in the fluorophore concentration (8). From a practical perspective, however, these methods also frequently suffer from low signal/noise ratios per trace, which means that averaging from multiple samples is generally required to accurately resolve kinetic parameters.

One of the main advantages of surface-based bioanalytical sensor technologies is that they offer the possibility of rapidly screening multiple recognition events either sequentially or simultaneously. In this approach, the same set of surface-immobilized probe molecules is exposed to a series of different compounds in an automated fashion. The emerging importance of these sensors in the field of life science stems from the fact that they can be combined with microfluidic handling (9), which makes them compatible with small sample volumes and thus ideally suited for studies of substances that are rare or time-consuming and expensive to obtain. Currently, surface plasmon resonance (SPR) is the predominant surface-based bioanalytical sensor. It is based on excitation of laterally propagating surface plasmons at planar metal (usually gold) substrates, where the condition for SPR excitation is extremely sensitive to changes in the interfacial refractive index, $\Delta n_{\text{interface}}$. Hence, by immobilizing probe molecules on the surface, one can monitor the binding of targets to the immobilized probes in real time via a response that, to a good approximation, is proportional to $\Delta n_{\text{interface}}$ (10,11).

In this work, we demonstrate the applicability of a recently published method (12) for measuring passive diffusion and membrane-protein-mediated transfer across membranes

Submitted October 13, 2009, and accepted for publication March 19, 2010.

*Correspondence: magnus.branden@chalmers.se or fredrik.hook@chalmers.se

Editor: Robert Nakamoto.

0006-3495/10/07/0124/10 $2.00

doi: 10.1016/j.bpj.2010.03.059

with an acquisition rate of 100 ms. The method is based on resolving the temporal change in the refractive index that occurs upon a transfer-dependent change in the solute concentration inside liposomes associated to a SPR active sensor surface, thus enabling the direct measurement of the transfer of a solute across lipid bilayers. To date, direct solute transport measurements have been obtained for charged molecules in studies using patch-clamp (13) or chip-based (14) technologies, but not, to our knowledge, for uncharged molecules. Here, we demonstrate screening of multiple permeation events by sequential measurements of glycerol, urea, and hydroxyurea permeabilities. Glycerol and urea are important cellular metabolites, and hydroxyurea is a drug that is widely used in cancer chemotherapy (15) as well as in treatment of HIV-virus infections (16). We also demonstrate the compatibility of the method for time-resolved monitoring of membrane-protein-mediated transfer by measuring the facilitated diffusion of sugar alcohols mediated by the aquaglyceroporin PfAQP from *Plasmodium falciparum*, the bacterial parasite responsible for malaria. This disease accounts for 300–500 million infections each year and causes ~2 million deaths annually (17). The increasing resistance of this parasite to current pharmaceuticals has intensified the search for new drug candidates or cocktails of inhibitors that may help alleviate this widespread human suffering. The genome of *P. falciparum* contains only a single member of the aquaporin family (PfAQP) (17), which facilitates the passive transport of both water and other small, uncharged molecules such as sugar alcohols. Since this aquaglyceroporin is believed to play an important role during the blood stage of the parasitic cycle (18), it shows promise as a potential drug target. The recently reported structure of PfAQP reveals the chemical nature of the channel in great detail (19), but the development and characterization of potential inhibitors targeting this membrane protein are hindered by the lack of reliable, high-throughput tools to screen the inhibition properties of candidate compounds. In this work, we demonstrate the high sensitivity, throughput, and reliability of the evanescent-wave-based assay by screening the permeability of sugar alcohols of various lengths at different temperatures in a single measurement and on the same set of immobilized liposomes. Analysis of the temperature dependence of the sugar permeability reveals that the activation energies for facilitated diffusion of xylitol and sorbitol are the same as that of the shortest sugar alcohol, glycerol, when transported through the homologous aquaglyceroporin of *Escherichia coli* (20).

MATERIALS AND METHODS

Liposome production

1-Palmitoyl2-oleoyl-*sn*-glycero-3-phophocholine (POPC) liposomes were made by first evaporating the solvent, chloroform, from the POPC lipids (from Avanti Polar Lipids, Alabaster, AL) using a flow of nitrogen gas. The dried lipids were then kept under vacuum overnight, after which 50 mM Tris(hydroxymethyl)aminomethane hydrochloride, 100 mM NaCl, pH 8.0 (Tris buffer) was added. The solution of dissolved POPC lipids (4 mg/mL) was then vortexed for ~10 min. Small unilamellar liposomes were made using a mini extruder (Avanti Polar Lipids) with polycarbonate membranes (pore size: 50 nm). *E. coli* liposomes were formed by sonication of *E. coli* polar lipid extract (Avanti Polar Lipids) as described previously (21). The lipids were sonicated (special ultrasonic cleaner; Laboratory Supplies Company, Hicksville, NY) at a concentration of 10 mg/mL to clarity in reconstitution buffer (50 mM Tris, pH = 8.0, 100 mM NaCl).

Production and purification of PfAQP

PfAQP was cloned, grown, and purified as described previously (22). Briefly, *Pichia pastoris* cells that heterologously overexpress a gene-optimized and C-terminally his_6-tagged construct were grown in a bioreactor in which protein production was induced with methanol. The obtained cells were disrupted using X-Press equipment (AB Biox, Gothenburg, Sweden) and the membranes were isolated by differential centrifugation. Solubilization of the protein was performed using 5% β-octylglucopyranoside (β-OG) from Anatrace, (Maumee, OH) which was also present at 1% during the subsequent Ni-NTA affinity purification and size exclusion chromatography. Finally, the protein was concentrated to 5 mg/mL using a 100,000 molecular weight cut-off Vivaspin column.

PfAQP reconstitution

The liposomes were first destabilized in 1.15% β-OG, followed by addition of purified PfAQP-protein at a concentration of ~5 mg/mL, which corresponds to a lipid/protein ratio (w/w) of 50. After incubation for 20 min, the suspension was diluted 35 times with reconstitution buffer. Finally, proteoliposomes were collected by ultracentrifugation (Beckmann type 45 Ti rotor, 145,000 *g*, 12 h, 4°C) and resuspended in reconstitution buffer at 4 mg/mL.

Surface modification

A carboxy-terminated gold chip was docked in a Biacore-2000 instrument. The carboxy-terminated gold surface was either a C1 chip or an Au chip that had been incubated overnight with 11-mercapto-undecanoic acid (both chips were purchased from GE Healthcare Life Sciences, Uppsala, Sweden). The running buffer was Tris buffer and the flow rate was set to 5 μL/min. NeutrAvidin (50 μg/mL; Invitrogen, Carlsbad, CA) was injected and covalently bound to the carboxy groups at the surface, which had been activated by means of an amine-coupling kit from GE Healthcare. Subsequently, 2 μM of biotin-DNA (a 15-base-long, single-stranded DNA that is covalently modified at one end with biotin) were injected, resulting in specific binding of the biotin moiety to NeutrAvidin. The biotin-modified DNA was dissolved in Tris buffer, and the NeutrAvidin was dissolved in 10 mM acetate, 150 mM NaCl, pH 4.7.

Measurements on transfer across liposomal membranes

Unilamellar liposomes (2 mg/mL lipid) and cholesterol-modified DNA (0.17 μM) were incubated for 30 min at room temperature, yielding approximately five DNA tags per liposome. The cholDNA-tag (Layerlab AB, Gothenburg, Sweden) has a 15-base-long sticky end and a 15-basepair-long duplex, at the end of which two cholesterol moieties are attached. After the cholesterol-modified DNA was incubated with liposomes, the cholesterol moieties were self-incorporated into the hydrophobic part of the lipid membrane. CholDNA-tagged liposomes (2 mg/mL of lipid concentration) were injected onto the functionalized sensor surface at a flow rate of 5 μL/min (the running buffer was Tris). The single-stranded sticky end of

the cholDNA-tag hybridized with the complementary single-stranded DNA immobilized on the sensor chip, resulting in attachment of the liposomes to the sensor surface. The permeable analytes were dissolved in running buffer and then sequentially injected until equimolar concentrations of the analyte were obtained inside and outside of the liposomes. Subsequently, the analyte-containing buffer was rapidly exchanged (~100 ms) for pure buffer, and the analyte molecules were then transferred out from the liposomes mediated by either passive or PfAQP-facilitated diffusion. The flow rate was 100–20 μL/min depending on the timescale of the recorded transfer event.

Calculation of sugar alcohol binding energies

Binding energies were calculated using AutoDock 4.2 (from AutoDock, La Jolla, CA) based on the structure of PfAQP (PDB entry: 3C02). AutoDockTools was used to add hydrogens, active torsions, and charges to the ligands as well as the protein, whose side chains were considered to be inflexible. Glycerol, xylitol, and sorbitol were docked using a Lamarckian genetic algorithm, starting from 300 random positions along the whole channel and parts of the intra- and extracellular vestibules (41 × 41 × 109 points, with a grid spacing of 0.375 Å). Further energy minimization of the conformations was performed for the 30 best positions. The results were ranked and clustered using the native scoring function of AutoDock.

RESULTS

SPR was used to monitor permeation across the lipid bilayer of liposomes that were gently immobilized onto the sensor surface. The SPR-active gold surface was first coated with NeutrAvidin, which is in complex with a biotin-modified, 15-base-long, single-stranded DNA. Liposomes were then bound to the surface through hybridization between the surface-immobilized DNA and complementary DNA strands attached via cholesterol anchors to the liposomes (12,23). (Note, however, that other means of liposome immobilization can be used as long as the integrity of the membrane is not altered.) Transfer measurements were performed as illustrated in Fig. 1. First, liposomes were loaded with analytes by exposing them to running buffer containing the analyte molecules until equimolar concentrations of the analyte were obtained inside and outside of the liposomes. Subsequently, the analyte-containing buffer was rapidly exchanged (~100 ms) for pure buffer, and the analyte molecules were then transferred out from the liposomes mediated by passive or PfAQP-facilitated diffusion. Consequently, the analyte concentration inside the liposomes decreased, resulting in a temporal reduction in the interfacial refractive index within the sensing volume probed by SPR.

Refractive-index-based sensing for transfer across liposome membranes

Fig. 2 *A* shows changes in the SPR response units (RU) upon 1), injection of biotin-DNA (2 μM) to a NeutrAvidin-functionalized gold surface (see Materials and Methods); 2), injection of cholesterol-DNA-modified POPC liposomes (lipid concentration: 2 mg/mL; ~3 cholesterol-DNA tags per liposome) with an average diameter of 71 nm determined from dynamic light scattering (DLS); and 3), sequential injections of the analytes glycerol, urea, and hydroxyurea.

Since glycerol, urea, and hydroxyurea are rapidly transferred (within seconds) across the liposome membrane, the response from the loading of the liposomes with analyte molecules corresponds to the change in the entire sensing volume, including the interior of the liposomes, but excluding the volume occupied by the lipid bilayer of the liposomes. The inset in Fig. 2 *A* shows a calibration plot of the glycerol injections, demonstrating a linear dependency of the response on the bulk analyte concentration and hence the accompanied change in the refractive index within the total sensing volume (see below). Fig. 2 *B* shows the final part of one of the glycerol injections (200 mM), including the decrease in the response as the injection is terminated by rapid injection of running buffer (the same solution used during the analyte injection, but lacking glycerol). The inset in Fig. 2 *B* shows an enlargement of the kinetic trace (*open circles*) from the point in time when the glycerol injection is terminated and glycerol starts to diffuse out from the liposomes (the *solid line* is a single exponential fit to the kinetic trace). Also shown in the inset in Fig. 2 *B* is a second trace (*dashed line*) showing the response to removal of glycerol from the sensing volume

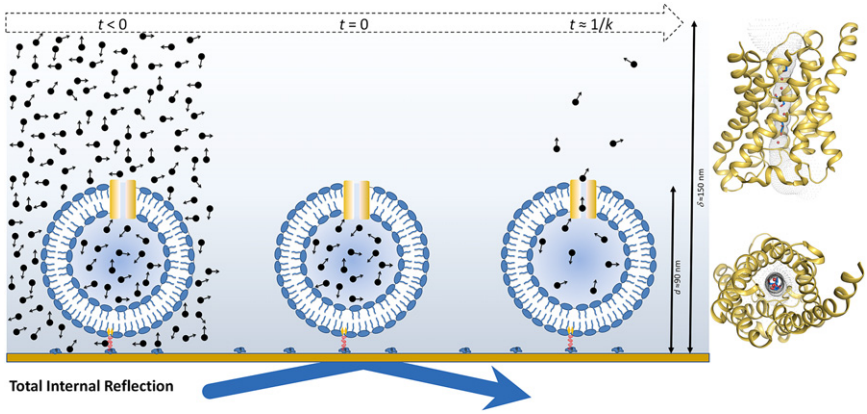

FIGURE 1 Left: Schematic illustration of PfAQP-reconstituted liposomes (diameter $d \approx$ 90 nm) immobilized within the evanescent fields (decay length, $\delta \approx$ 150 nm) of an SPR sensor surface. The sensing volume is first filled with the analyte molecules, yielding equimolar concentration inside and outside the liposomes ($t < 0$). The sensing volume is then rapidly exchanged to a solution containing no analytes ($t = 0$), leading to PfAQP-mediated transfer of the analyte out from the interior of the liposomes ($t \approx 1/k$, were k is the transfer rate constant). Right: A cartoon of PfAQP generated from the crystal structure (19) and viewed from the side and top with respect to the plane of the lipid bilayer membrane.

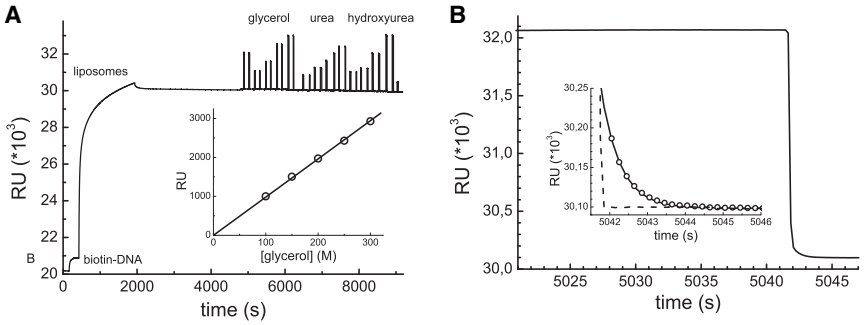

FIGURE 2 Refractive-index-based sensing of permeation using SPR. (*A*) The response from sequential injection of biotin-DNA, cholesterol-DNA-tagged POPC liposomes, and glycerol, urea, and hydroxyurea dissolved in running buffer (Tris). The inset in panel *A* shows a calibration curve generated from the glycerol injections, which illustrates the linear dependency of the response on the bulk analyte (glycerol) concentration in the entire sensing volume. (*B*) The termination of one of the 200 mM glycerol injections. At the point in time when the injection is terminated, there is a rapid time-unresolved decrease in RU, representing exchange of the measuring cell volume from a solution (Tris buffer) containing 200 mM glycerol to an identical solution containing no glycerol. The time-unresolved step is followed by a slower decrease, which is rate-limited by the glycerol permeability of the liposome membrane. The inset in panel *B* shows an enlargement of the kinetic trace representing permeation of glycerol out of the liposomes (*circles*) fitted to a single exponential curve (*solid line*). Also included in the figure is a kinetic trace (*dashed line*) after the termination of a 200 mM glycerol injection to a sensor surface without attached liposomes (i.e., a negative control).

after termination of an identical glycerol injection pulse to a sensor surface without attached liposomes. This provides a negative control showing that the kinetic trace (*open circles* in Fig. 2 *B*) does not result from analyte interaction with the underlying sensor surface. Fig. 2 *B* shows that the release of glycerol was well represented by a single exponential function with a rate constant of 1.7 s^{-1}, which converts (see below) to a glycerol permeability that is in good agreement with expectations (24). The amplitude (R_L = 189 RU) of the response corresponds to the refractive index of glycerol within the nonleaky fraction of surface-attached liposomes, which is quantified in the next section.

Quantification of the integrity of surface-immobilized liposomes

With the SPR technique, in contrast to time-resolved light-scattering studies, the fraction of the liposomes that contribute to the response can be quantified and determined from the ratio between the response to release of analytes from the liposomes (R_L = 189 RU) and the total response to removal of analytes from the entire sensing volume (R_{tot} = 1970 RU). The surface-attached liposomes are located in the segment of the sensing volume closest to the surface, defined by the diameter of the liposome. For the SPR setup used in this work, the intensity of the evanescent field decays exponentially from the sensor surface with a decay length, δ, of ~150 nm (see Fig. 1). This means that the measured response, R_d, from a change in bulk refractive index within a segment defined by the liposome film thickness, d, will relate to the response upon an identical change in bulk refractive index of the total sensing volume, R_∞, as (10):

$$R_d = R_\infty \frac{\int_0^d e^{-z/\delta} dz}{\int_0^\infty e^{-z/\delta} dz} = R_\infty \left(1 - e^{-d/\delta}\right) \quad (1)$$

The ratio between R_L and R_{tot} can be represented by:

$$\frac{R_L}{R_{tot}} = \frac{R_d(\alpha_l - \alpha_{l.b.})}{R_\infty - \alpha_{l.b.} \times R_d} \quad (2)$$

where α_l and $\alpha_{l.b}$ are the liposome and the lipid bilayer fractions, respectively, of a sensing segment with thickness, d. Combining Eqs. 1 and 2 thus yields:

$$\frac{R_L}{R_{tot}} = \frac{\left(1 - e^{-d/\delta}\right)(\alpha_l - \alpha_{l.b.})}{1 - \alpha_{l.b.}\left(1 - e^{-d/\delta}\right)} \quad (3)$$

With a mean diameter of the POPC-liposomes (produced by extrusion through a 50 nm filter) of ~71 nm (determined by DLS) and a lipid bilayer thickness of ~4 nm (25), $\alpha_{l.b} = 0.3 \times \alpha_l$. Inserting the values for R_L and R_{tot} into Eq. 3 yields α_l = ~0.33, which corresponds to a surface coverage of nonleaky liposomes of ~50%. This coverage is in very good agreement with the theoretical value of 54% for random sequential adsorption of spheres (26), indicating that the measured release is determined by the change in refractive index of the interior solution of essentially the entire population of immobilized liposomes. Moreover, since the decrease in RU upon transfer of analytes out of the liposomes corresponds well to the theoretical value, these findings also suggest that the contribution from fluctuations in the size of the liposomes to the measured response is negligible, in agreement with the fact that liposomes below a diameter of ~80 nm are osmotically noncompressible (<1%) (27). This insensitivity to changes in liposome size provides a significant practical advantage for measuring facilitated diffusion of uncharged solutes over lipid bilayers, as opposed to conventional light-scattering approaches that detect changes in liposome size due to both water and solute transport. Thus, the technically challenging requirement that osmolarities must be balanced both inside and outside of liposomes in isoosmotic-solution swelling assays (28) is completely side-stepped by this direct approach to assaying membrane transport.

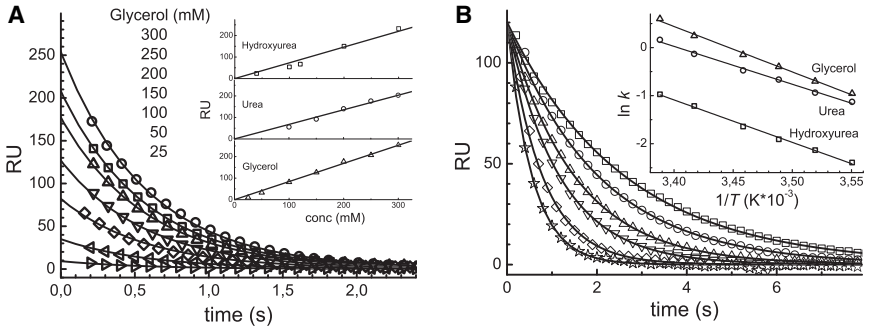

FIGURE 3 (*A*) The dependence of glycerol permeation on the concentration gradient across the liposome membrane, at $T = 22°C$. The kinetic traces in the concentration series were globally fitted to single exponential curves (*solid lines*) with a common rate constant of $R^2 = 0.999$. The insets demonstrate the linear dependency of the amplitude on the concentration gradient of glycerol (*triangles*), urea (*circles*), and hydroxyurea (*squares*) across the liposome membrane. (*B*) The dependence of glycerol permeation on the temperature. The kinetic traces were fitted to single exponential curves (*solid lines*). The inset shows linear fits (*solid lines*) of ln(k) versus $1/T$, obtained for glycerol, urea, and hydroxyurea, yielding the permeation activation energies, E_{act}, with $R^2 = 0.996$ (for glycerol), 0.994 (for urea), and 0.996 (for hydroxyurea).

Passive diffusion across lipid membranes

Passive diffusion of glycerol, urea, and hydroxyurea was determined by measuring the rate of efflux of these analytes from the liposomes. Fig. 3 *A* shows the concentration dependence of the rate of passive diffusion of glycerol. The concentration dependence for glycerol, urea (not shown), and hydroxyurea (not shown), at $T = 22°C$, could all be represented with common rate constants ($k_{glycerol} = 1.75 \pm 0.02\ s^{-1}$ ($n = 7$), $k_{urea} = 1.23 \pm 0.06\ s^{-1}$ ($n = 10$), and $k_{hydroxyurea} = 0.359 \pm 0.004\ s^{-1}$ ($n = 7$)), with amplitudes that scale linearly with the concentration gradient of the different analytes (shown for glycerol, urea, and hydroxyurea in the *inset* in Fig. 3 *A*). These results are in agreement with passive diffusion across a lipid bilayer, which is a thermodynamically irreversible process described by a first-order rate constant that is independent of, and an amplitude that is linearly dependent on, the concentration gradient of the permeable analyte. For passive diffusion, the flow rate, J (mole×cm^{-2}×s^{-1}), of permeable analytes across the lipid bilayer can be described by Fick's law as:

$$J = P\Delta C \tag{4}$$

where ΔC (mole/cm^3) is the solute concentration gradient across the membrane and P (cm/s) is the permeability coefficient, which depends on the observed rate constant, k, according to:

$$P = kVS^{-1} = k\frac{r}{3} \tag{5}$$

where V (cm^3) is the volume, S (cm^2) is the inner surface area, and r is the inner radius of the liposome. With a mean diameter of the liposomes of ~71 nm and a lipid bilayer thickness of ~4 nm (25), the permeability coefficients for the three permeants (glycerol, urea, and hydroxyurea) at 22°C then become 1.84×10^{-6}, 1.29×10^{-6}, and 0.38×10^{-6} cm/s, respectively. These values are in good agreement with previous studies on the permeability of glycerol (2.1×10^{-6} cm/s) (24) and urea (1.3×10^{-6} cm/s) (29) across POPC lipid bilayers. The linear dependency of k on r^{-1} was confirmed by repeating the experiment using liposomes with a diameter of 93 nm, yielding $k_{glycerol}$ (93 nm) = 1.46 s^{-1} (data not shown), which is in good agreement with the expected value of 1.3 s^{-1}.

Besides the ability to rapidly determine membrane permeability by subsequent additions of different analytes to the very same set of immobilized liposomes, the method also allows the temperature to be varied within a single experiment, thus providing a thermodynamic characterization of the transfer reactions. Fig. 3 *B* shows the temperature dependence of the rate of passive diffusion of glycerol across the liposome membrane, and the inset shows a plot of ln(k) versus $1/T$ for glycerol, urea, and hydroxyurea according to the Arrhenius equation:

$$\ln(k) = \ln(A) - \frac{E_{act}}{RT} \tag{6}$$

where A is the preexponential factor, T (K) is the absolute temperature, R (kcal×mole^{-1}×K^{-1}) is the universal gas constant, and E_{act} (kcal×mole^{-1}) is the activation energy.

Fits to the curves in the inset of Fig. 3 *B* using Eq. 6 yield E_{act} (kcal×mole^{-1}) values of 18.8 ± 1.3 ($n = 6$), 15.7 ± 1.3 ($n = 6$), and 17.5 ± 1.1 ($n = 6$) for passive diffusion of glycerol, urea, and hydroxyurea, respectively. These values are slightly higher than corresponding literature values obtained from diffusion across egg-lecithin bilayers (11.0, 9.3, and 10.9 kcal×mole^{-1}, respectively) (29,30). Most likely, these differences reflect the difference in lipid composition, which is known to influence the permeability (31). Note, however, that the relative differences in the magnitude of E_{act} for hydroxyurea, urea, and glycerol are essentially identical to those obtained in a previous study (30). As previously suggested (30,32), this relative difference in activation energy is attributed to differences in dehydration energy upon transfer of the analyte molecules from a hydrated state in the aqueous phase to a dehydrated state in the hydrophobic part of the lipid bilayer, which correlates well with the ability of the analyte molecules to form hydrogen bonds with water.

Membrane-protein mediated transfer across lipid membranes

To demonstrate the applicability of this method to study and elucidate the mechanistic details of membrane-protein mediated transfer, we investigated facilitated diffusion of sugar alcohols mediated by the aquaglyceroporin PfAQP from *P. falciparum* reconstituted into liposomes made of lipid extract from *E. coli*. Fig. 4 *A* demonstrates how, in a single set of immobilized reconstituted liposomes, the transfer of several analytes (sugar alcohols) can be sequentially monitored at several different temperatures to obtain the permeability coefficients and activation energies of facilitated diffusion in a single experiment. Fig. 4 *B* shows the kinetic traces that describe the release, at 23°C, of xylitol (400 mM) from liposomes without (*black*) and with reconstituted PfAQP (*red*), respectively. The trace corresponding to PfAQP-reconstituted liposomes is characterized by two clearly visible kinetic components. Under the assumption that facilitated diffusion is much faster than passive diffusion, the fast component can be attributed to facilitated diffusion in liposomes containing PfAQP, whereas the slow component, which exhibits the same rate as that observed for nonreconstituted liposomes, can be attributed to passive diffusion of xylitol in a fraction of reconstituted liposome population containing no functional PfAQP. A fraction of reconstituted liposomes containing no membrane protein is commonly observed (21) when the same reconstitution protocol used here is employed. The fraction of liposomes containing no functional PfAQP, $F(n = 0)$, could be estimated to 0.36 from a comparison of the relative amplitude of passive diffusion of glycerol in reconstituted and nonreconstituted liposomes (Fig. 4 *C*). Note that facilitated diffusion of glycerol cannot be resolved with the time resolution (~100 ms) of our setup, and hence only the passive diffusion of glycerol in the fraction of reconstituted liposomes containing no functional transporters is recorded and observed in Fig. 4 *C*.

Under the assumption that the number (n) of PfAQP per liposome is Poisson-distributed, the estimation of $F(n = 0) = 0.36$ gives a mean number (m) of PfAQP per liposome of 1.016, with $F(n = 1) = 0.368$, $F(n = 2) = 0.188$, $F(n = 3) = 0.064$, $F(n = 4) = 0.016$, and $F(n > 4) = 0.004$. The inset of Fig. 4 *B* shows an enlargement of the fast component describing facilitated diffusion of xylitol by PfAQP, including a fit to the following expression:

$$A = F(n = 1)A_0e^{-kt} + F(n = 2)A_0e^{-2kt} + F(n = 3)A_0e^{-3kt} + F(n = 4)A_0e^{-4kt} \quad (7)$$

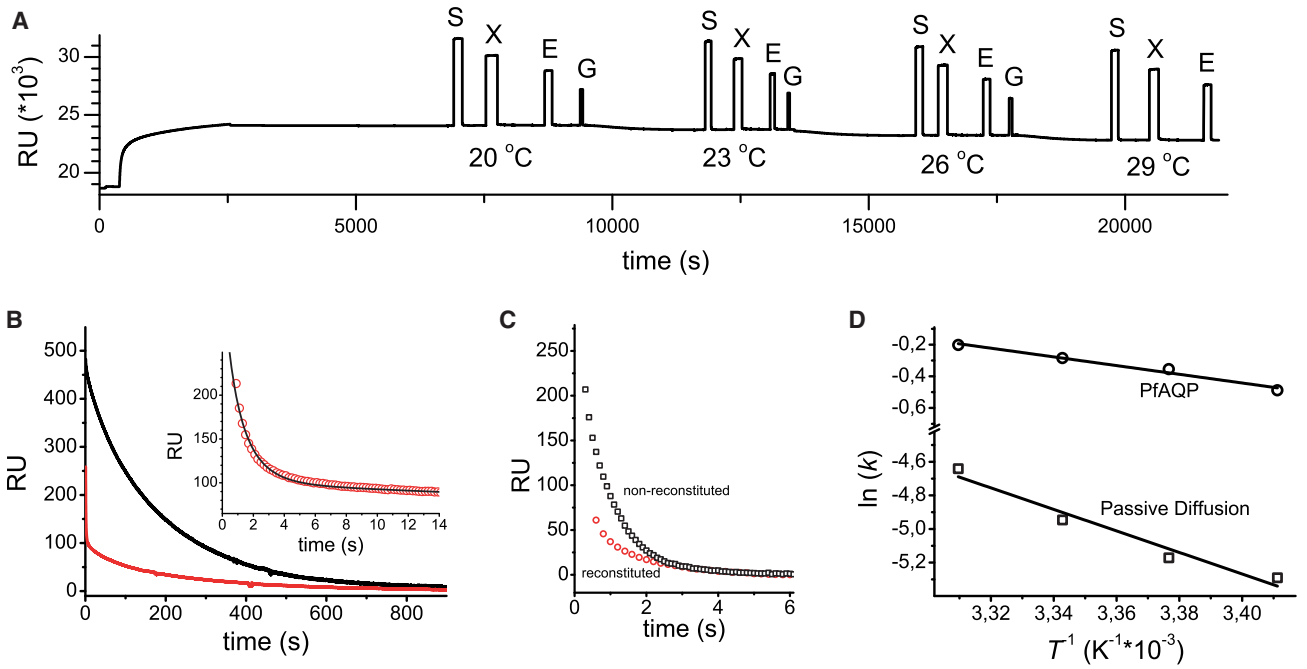

FIGURE 4 (*A*) Screening of facilitated diffusion in PfAQP-reconstituted liposomes of sorbitol (S), xylitol (X), erythritol (E), and glycerol (G) at temperatures of 20°C, 23°C, 26°C, and 29°C. (*B*) Measurement, at 23°C, of xylitol (400 mM) release from liposomes made from *E. coli* lipid extract. The red trace shows release from PfAQP-reconstituted liposomes. The black trace shows release from liposomes prepared in the same way as those used to generate the red dashed trace, but without the addition of PfAQP in the reconstitution step. The kinetic trace in red has two clearly distinguishable components: one slow, with the same rate as that of the black trace, representing passive diffusion of xylitol in liposomes containing no PfAQP, and one fast component representing facilitated diffusion of xylitol in liposomes containing PfAQP. The inset shows an enlargement of the fast component fitted to Eq. 7 (see main text) yielding the black solid line and the rate constant, k, for facilitated diffusion. (*C*) A comparison of passive diffusion of glycerol in nonreconstituted liposomes and in the fraction of reconstituted liposomes containing no functional transporters, respectively. (*D*) Linear fits (*solid lines*) of ln(k) versus $1/T$, with rate constants for facilitated and passive diffusion of xylitol obtained from measurements on reconstituted and nonreconstituted liposomes, respectively.

where $F(n)$ is the preestimated (see above) fraction of liposomes containing $n = 1$–4 functional PfAQP per liposome (the contribution from $F(n > 4)$ to the kinetic trace is negligible and therefore not included in Eq. 7), and A_0 and k are the only two unknown parameters, corresponding to the amplitude of the total response and the rate constant of facilitated diffusion in liposomes containing one functional PfAQP, respectively. Hence, a fit of the fast component in the inset of Fig. 4 *B* to Eq. 7 yields a rate constant for facilitated diffusion of xylitol in liposomes containing one PfAQP ($k_{xyl,AQP}$), at 23°C, of 0.70 s^{-1} ± 0.02 ($R^2 = 0.998$). The corresponding rate constant for passive diffusion of xylitol ($k_{xyl,P.D}$), at 23°C, measured on nonreconstituted liposomes is 5.7×10^{-3} s^{-1} ± 5×10^{-6} ($R^2 = 0.998$). Given a liposome inner radius of 44.6 nm measured using DLS (data not shown), the permeabilities for facilitated and passive diffusion can be estimated using Eq. 5 to 1.04×10^{-6} cm/s ($P_{xyl,AQP}$) and 8.47×10^{-9} cm/s ($P_{xyl,P.D}$), respectively.

Identical analyses of the measured rate constants of both passive and facilitated diffusion at various temperatures yielded the plots shown in Fig. 4 *D* of ln(k) versus 1/T. Linear fits (Fig. 4 *D*, *solid lines*) of these plots gave the activation energies $E_{act,xyl,AQP} = 5.5 \pm 0.5$ kcal/mol ($n = 4$, $R^2 = 0.97$) and $E_{act,xyl,p.d.} = 12.8 \pm 1.8$ kcal/mol ($n = 4$, $R^2 = 0.94$) for facilitated and passive diffusion, respectively. Hence, facilitated diffusion lowers the activation energy for transfer of xylitol across the membrane by a factor of 2.3. Analysis of the facilitated diffusion of sorbitol and erythritol, measured on the same set of immobilized liposomes as used for the xylitol measurements (Fig. 4 *A*), gave the following values for sorbitol: $P_{sorb,AQP} = 1.09\times10^{-7}$ cm/s (at 23°C) and $E_{act,sorb,AQP} = 5.6 \pm 0.3$ kcal/mol ($n = 4$, $R^2 = 0.99$). For erythritol, the rate of facilitated diffusion was on the limit of which could be time-resolved (only the last few data points were time-resolved), allowing for an estimate of $P_{eryth,AQP} \approx 3\times10^{-6}$ cm/s (at 23°C), but not for a determination of the rate's temperature dependency and the extraction of $E_{act,eryth,AQP}$.

DISCUSSION

In this study, we have extended the scope of application of a recently developed method for directly monitoring the transfer of uncharged molecules across a lipid membrane bilayer (12) to study passive and membrane-protein facilitated diffusion of uncharged solutes. In contrast to conventional light-scattering and fluorescence-quenching methods, which require that permeability measurements be performed on samples in suspension, the SPR-based method offers advantages inherent to surface-based analytical tools. One important example of the advantage of surface immobilization of liposomes, which so far has been explored for use in measuring solute exchange over lipid bilayer membranes using fluorescent microscopy (33–35), is that it provides compatibility with multiple measurements of different analytes on the very same sample of liposomes (Figs. 2 and 4) without the signal-intensity reduction caused by fluorophore bleaching. Furthermore, since sample injection is automated, the method is ideally suited for screening a drug candidate's ability to penetrate cellular membranes or its influence on membrane-protein-mediated transfer.

It is also worth emphasizing that the ability to perform multiple measurements on the same set of immobilized liposomes greatly reduces the sample consumption compared to conventional stopped-flow techniques in which the transfer rate is obtained from averaging multiple measurements, each on a new sample of liposomes. This feature is especially desirable for studies of proteoliposomes, since both membrane-protein purification and reconstitution into liposomes are time-consuming and expensive processes that frequently result in limited amounts of active protein. For comparison, using a conventional stopped-flow technique, a measurement of aquaporin activity typically requires 10 recordings of the transport event, which are averaged and fitted to obtain the transfer rate constant. This corresponds to a consumption of 400 μg of membrane protein (21,36). In this study, 8 μg of PfAQP were consumed in the liposome-immobilizing step by injecting 200 μL of reconstituted liposomes. However, this amount could be reduced by at least one order of magnitude by either halting the flow or reusing the sample by looping it back to the sensor surface, instead of wasting the liposome sample passing the sensor surface. More importantly, the same set of immobilized liposomes can be used to measure multiple transfer events. In this study, we used the same set of immobilized reconstituted liposomes for 1 day (~12 h) of measurements with no loss of functionality. In a screening study, this could easily correspond to >100 transfer events being monitored with <8 μg of protein being consumed. With conventional stopped-flow techniques, the corresponding value can be estimated to be >40 mg of consumed protein.

Another unique aspect of this approach is that it enables a straightforward quantification of facilitated diffusion per membrane protein and membrane area. Hence, from the above calculated values of $P_{xyl,AQP}$ and $P_{xyl,P.D}$, where $P_{xyl,AQP}$ can be said to represent the increase in permeability per PfAQP and membrane area, the membrane surface concentration of PfAQP that is required to up-regulate (an increase of the uptake rate above that accounted for by passive diffusion) the transfer of xylitol can be determined to ~1 AQP per μm^2. Hence, up-regulation occurs at a surface concentration of ~1 PfAQP per μm^2 of membrane surface, or at a concentration of as few as 1 to 100 PfAQP molecules for cells with typical diameters in the range of 1–10 μm. Furthermore, the pore radius of PfAQP at its point of entry has been estimated from its crystal structure to be ~0.6 nm (19). Given this radius, the specific xylitol permeability of the PfAQP can be calculated to be 2.3×10^{-2} cm/s using Eq. 5, where S is now the surface area of the pore opening and V is the volume of the liposome. These specific values on the permeability of

facilitated diffusion could not be obtained in previous studies using conventional stopped-flow techniques (37,38), and (only) relative values for facilitated diffusion of sugar alcohols could be compared due to the lack of information on the number of PfAQPs present within, and the integrity of, the lipid membrane.

In aqueous solutions, solutes, like sugar alcohols, form hydrogen-bond interactions with surrounding water molecules, and the activation energies for passive diffusion across the lipid bilayers reflect their solvent dehydration energies. An aquaglyceroporin thus facilitates (i.e., lowers the activation energy for) diffusion by providing a hydrogen-bond network to the sugar alcohol within its pore, thereby compensating for the solute's loss of hydrogen bonds to water molecules as it enters the channel. Whereas the activation energies for facilitated water transport of the wild-type PfAQP has been determined as 3.5 kcal/mol, which increases to 7.5 kcal/mol in the E125S PfAQP mutant (37), we are not aware of any previous measurements of the activation energies of PfAQP for facilitated transport of sugar alcohols, nor any determination of facilitated transport activation energies for any long-chain sugar alcohol for any aquaglyceroporin. Our determinations of the energies of activation for facilitated diffusion of xylitol and sorbitol show them to be identical within experimental uncertainty (5.5 $\pm$ 0.5 kcal/mol and 5.6 $\pm$ 0.3 kcal/mol, respectively), and these values show surprisingly high agreement with an earlier measurement of the activation energy (4.5 kcal/mol) of glycerol transport through the aquaglyceroporin GlpF of *E. coli* (20).

Molecular-dynamics simulations have repeatedly shown that the major energetic barrier to glycerol transport through GlpF lies near the conserved aromatic/arginine (ar/R) selectivity filter (39–41), and that the energetic cost of passing a solute across the selectivity filter results from the breaking of favorable interactions between the selectivity filter and the water molecules therein (40). Hence, the activation energy for facilitated diffusion through the pore is the sum of the energetic cost of removing the water molecules and the energy gained from the interaction made by the permeating solute with the selectivity filter. Therefore, calculations of the binding energies of glycerol, xylitol, and sorbitol to the ar/R region of the PfAQP structure (19) using Autodock could provide an indication of the ar/R region's selectivity toward these sugar alcohols. From such an analysis, we obtained binding energy estimates of -3.7 kcal/mol for glycerol and -4 kcal/mol for xylitol and sorbitol when docked near a conserved ar/R selectivity filter (Fig. 5).

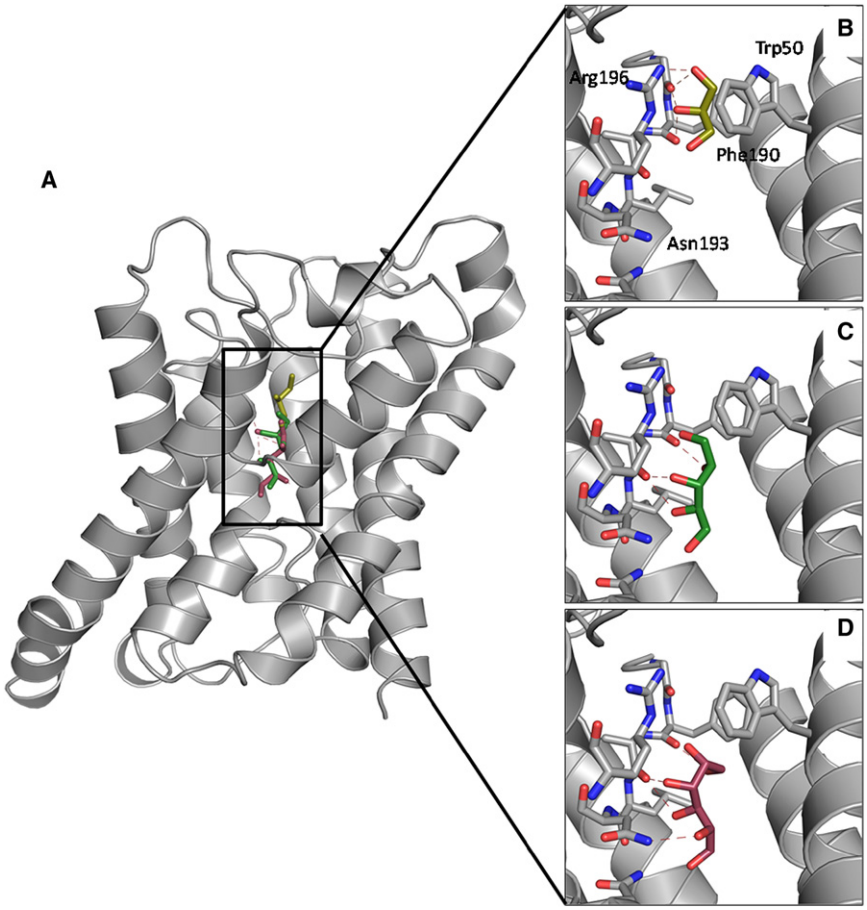

FIGURE 5 Illustrations of (*A*) the PfAQP crystal structure, obtained from the PDB entry 3C02 (19), and docking of (*B*) glycerol, (*C*) xylitol, and (*D*) sorbitol to the ar/R-selectivity filter of PfAQP determined by AutoDock. Hydrogen bonds (distance < 3.0 Å) are shown in red as dashed lines.

Despite the similar activation energies, we observed significant differences in the substrate transport rates, with glycerol transport being too fast to quantify ($P_{AQP} > 1\times10^{-5}$ cm/s), and the permeability for erythritol ($P_{AQP} = 3\times10^{-6}$ cm/s) being larger than that of xylitol ($P_{AQP} = 1\times10^{-6}$ cm/s), which in turn was larger than that of sorbitol ($P_{AQP} = 1\times10^{-7}$ cm/s), as was also observed in previous studies (37,38). Since the measured activation energies were independent of length, these kinetic differences must be explained as resulting from differences in the preexponential factor A (Eq. 6), which describes the frequency of successful collisions in a bimolecular reaction. Thus, the rate constant for facilitated transport of a specific sugar alcohol also depends upon the frequency with which it successfully collides with the pore entrance. This factor will clearly be influenced by steric considerations since long-chain sugar alcohols must collide not only with the pore entry, but also with the right orientation. Hence, our observation that the activation energy, but not the preexponential factor, is independent of the sugar alcohol size is in excellent agreement with previous results from molecular-dynamics simulations (40) indicating that the rate of solute passage through the aquaglyceroporin pore is determined not by water-solute interactions, but by water-selectivity filter interactions and steric effects.

Finally, for fast transfer events, such as those mediated by certain membrane proteins, conventional (indirect) stopped-flow based methods are limited by the fact that water permeation does not occur significantly faster than analyte transfer. In such cases, water transfer will lag behind the analyte transfer, and thus the analyte transfer rate cannot be obtained from a simple analysis of the change in liposome size. In fact, knowledge of the rate of water transfer is a prerequisite in these cases and must be obtained from separate control experiments. In contrast, the SPR-based method is independent of the rate of water transfer since the redistribution of water molecules across the liposomal membrane does not contribute to the measured response, and the influence of swelling or shrinkage of the immobilized liposomes is insignificant for small liposomes. Although the time resolution (~100 ms) of the setup used in this study is insufficient for resolving very fast transfer events, such as facilitated diffusion of glycerol, significant improvements in the time resolution of this methodological approach are considered technically realizable. Combining label-free plasmonic readouts for small areas (42) with rapid mixing using microfluidic concepts (43) should improve both the acquisition rate and the microfluidic-controlled liquid exchange to push the detection limit into the submillisecond regime. We therefore believe that, given their compatibility with automatization, miniaturization, sample reduction, and parallel readout array formats, evanescent-wave sensing techniques (here illustrated using SPR) have a generic potential for facilitating functional studies of membrane-protein-mediated transfer of not only nonelectrolytes, but of any analyte (including D_2O and ions) with a refractive index different from that of water.

This work was financially supported by an Ingvar Grant from the Swedish Strategic Research Foundation, Layerlab AB, the European Commission FP7 program ASMENA, the FP7 Integrated Project EDICT, the FP7 Marie Curie Research Training Network Aqua(glycero)porins, Vinnova, and the Swedish Science Research Council (V.R.).

REFERENCES

1. Bangham, A. D. 1968. Membrane models with phospholipids. *Prog. Biophys. Mol. Biol.* 18:29–95.
2. Borgnia, M. J., and P. Agre. 2001. Reconstitution and functional comparison of purified GlpF and AqpZ, the glycerol and water channels from *Escherichia coli*. *Proc. Natl. Acad. Sci. USA.* 98:2888–2893.
3. Manley, D. M., M. E. McComb, …, J. D. O'Neil. 2000. Secondary structure and oligomerization of the *E. coli* glycerol facilitator. *Biochemistry.* 39:12303–12311.
4. Cohen, B. E., and A. D. Bangham. 1972. Diffusion of small non-electrolytes across liposome membranes. *Nature.* 236:173–174.
5. Verkman, A. S. 1995. Optical methods to measure membrane transport processes. *J. Membr. Biol.* 148:99–110.
6. Levitt, D. G., and H. J. Mlekoday. 1983. Reflection coefficient and permeability of urea and ethylene glycol in the human red cell membrane. *J. Gen. Physiol.* 81:239–253.
7. Chen, P. Y., and A. S. Verkman. 1987. Non-electrolyte transport across renal proximal tubule cell membranes measured by tracer efflux and light scattering. *Pflugers Arch.* 408:491–496.
8. Chen, P. Y., D. Pearce, and A. S. Verkman. 1988. Membrane water and solute permeability determined quantitatively by self-quenching of an entrapped fluorophore. *Biochemistry.* 27:5713–5718.
9. Jönsson, U., L. Fägerstam, …, M. Malmqvist. 1991. Real-time biospecific interaction analysis using surface plasmon resonance and a sensor chip technology. *Biotechniques.* 11:620–627.
10. Jung, L. S., C. T. Campbell, …, S. S. Yee. 1998. Quantitative interpretation of the response of surface plasmon resonance sensors to adsorbed films. *Langmuir.* 14:5636–5648.
11. Liedberg, B., I. Lundstrom, and E. Stenberg. 1993. Principles of biosensing with an extended coupling matrix and surface-plasmon resonance. *Sens. Actuators B Chem.* 11:63–72.
12. Brändén, M., S. Dahlin, and F. Höök. 2008. Label-free measurements of molecular transport across liposome membranes using evanescent-wave sensing. *ChemPhysChem.* 9:2480–2485.
13. Neher, E., and B. Sakmann. 1976. Single-channel currents recorded from membrane of denervated frog muscle fibres. *Nature.* 260:799–802.
14. Janshoff, A., and C. Steinem. 2006. Transport across artificial membranes—an analytical perspective. *Anal. Bioanal. Chem.* 385:433–451.
15. Fausel, C. 2007. Targeted chronic myeloid leukemia therapy: seeking a cure. *Am. J. Health Syst. Pharm.* 64(24, Suppl 15):S9–S15.
16. Lori, F., A. Foli, …, J. Lisziewicz. 2007. Virostatics: a new class of anti-HIV drugs. *Curr. Med. Chem.* 14:233–241.
17. Gardner, M. J., N. Hall, …, B. Barrell. 2002. Genome sequence of the human malaria parasite *Plasmodium falciparum*. *Nature.* 419:498–511.
18. King, L. S., D. Kozono, and P. Agre. 2004. From structure to disease: the evolving tale of aquaporin biology. *Nat. Rev. Mol. Cell Biol.* 5:687–698.
19. Newby, Z. E., J. O'Connell, 3rd, …, R. M. Stroud. 2008. Crystal structure of the aquaglyceroporin PfAQP from the malarial parasite *Plasmodium falciparum*. *Nat. Struct. Mol. Biol.* 15:619–625.
20. Maurel, C., J. Reizer, …, M. H. Saier, Jr. 1994. Functional characterization of the *Escherichia coli* glycerol facilitator, GlpF, in *Xenopus* oocytes. *J. Biol. Chem.* 269:11869–11872.
21. Nyblom, M., F. Oberg, …, K. Hedfalk. 2007. Exceptional overproduction of a functional human membrane protein. *Protein Expr. Purif.* 56:110–120.

22. Hedfalk, K., N. Pettersson, …, E. Gordon. 2008. Production, characterization and crystallization of the *Plasmodium falciparum* aquaporin. *Protein Expr. Purif.* 59:69–78.

23. Pfeiffer, I., and F. Höök. 2004. Bivalent cholesterol-based coupling of oligonucletides to lipid membrane assemblies. *J. Am. Chem. Soc.* 126:10224–10225.

24. Peterlin, P., and V. Arrigler. 2008. Electroformation in a flow chamber with solution exchange as a means of preparation of flaccid giant vesicles. *Colloids Surf. B Biointerfaces.* 64:77–87.

25. Wiener, M. C., and S. H. White. 1992. Structure of a fluid dioleoylphosphatidylcholine bilayer determined by joint refinement of x-ray and neutron diffraction data. III. Complete structure. *Biophys. J.* 61:434–447.

26. Hinrichsen, E. L., J. Feder, and T. Jossang. 1986. Geometry of random sequential adsorption. *J. Stat. Phys.* 44:793–827.

27. Sun, S. T., A. Milon, …, Y. Nakatani. 1986. Osmotic swelling of unilamellar vesicles by the stopped-flow light-scattering method—elastic properties of vesicles. *Biochim. Biophys. Acta.* 860:525–530.

28. Promeneur, D., Y. Liu, …, N. Kumar. 2007. Aquaglyceroporin PbAQP during intraerythrocytic development of the malaria parasite *Plasmodium berghei*. *Proc. Natl. Acad. Sci. USA.* 104:2211–2216.

29. Lande, M. B., J. M. Donovan, and M. L. Zeidel. 1995. The relationship between membrane fluidity and permeabilities to water, solutes, ammonia, and protons. *J. Gen. Physiol.* 106:67–84.

30. Cohen, B. E. 1975. The permeability of liposomes to nonelectrolytes. I. Activation energies for permeation. *J. Membr. Biol.* 20:205–234.

31. Disalvo, E. A., and S. A. Simon. 1995. Permeability and Stability of Lipid Bilayers. GRC, Boca Raton.

32. Stein, W. D. 1967. The Movement of Molecules Across Cell Membranes. Academic Press, New York.

33. Christensen, S. M., and D. Stamou. 2007. Surface-based lipid vesicle reactor systems: fabrication and applications. *Soft Matter.* 3:828–836.

34. Kuyper, C. L., J. S. Kuo, …, D. T. Chiu. 2006. Proton permeation into single vesicles occurs via a sequential two-step mechanism and is heterogeneous. *J. Am. Chem. Soc.* 128:3233–3240.

35. Stamou, D., C. Duschl, …, H. Vogel. 2003. Self-assembled microarrays of attoliter molecular vessels. *Angew. Chem. Int. Ed. Engl.* 42:5580–5583.

36. Fischer, G., U. Kosinska-Eriksson, …, K. Lindkvist-Petersson. 2009. Crystal structure of a yeast aquaporin at 1.15 angstrom reveals a novel gating mechanism. *PLoS Biol.* 7:e1000130.

37. Beitz, E., S. Pavlovic-Djuranovic, …, J. E. Schultz. 2004. Molecular dissection of water and glycerol permeability of the aquaglyceroporin from *Plasmodium falciparum* by mutational analysis. *Proc. Natl. Acad. Sci. USA.* 101:1153–1158.

38. Hansen, M., J. F. Kun, …, E. Beitz. 2002. A single, bi-functional aquaglyceroporin in blood-stage *Plasmodium falciparum* malaria parasites. *J. Biol. Chem.* 277:4874–4882.

39. Hénin, J., E. Tajkhorshid, …, C. Chipot. 2008. Diffusion of glycerol through *Escherichia coli* aquaglyceroporin GlpF. *Biophys. J.* 94:832–839.

40. Hub, J. S., and B. L. de Groot. 2008. Mechanism of selectivity in aquaporins and aquaglyceroporins. *Proc. Natl. Acad. Sci. USA.* 105:1198–1203.

41. Jensen, M. O., S. Park, …, K. Schulten. 2002. Energetics of glycerol conduction through aquaglyceroporin GlpF. *Proc. Natl. Acad. Sci. USA.* 99:6731–6736.

42. Dahlin, A. B., S. Chen, …, F. Höök. 2009. High-resolution microspectroscopy of plasmonic nanostructures for miniaturized biosensing. *Anal. Chem.* 81:6572–6580.

43. Sachs, F. 1999. Practical limits on the maximal speed of solution exchange for patch clamp experiments. *Biophys. J.* 77:682–690.